Noncontact Measurements of Sound Absorption Coefficient with a Pressure-velocity Probe, a Laser Doppler Vibrometer, and a Microphone Array

Leonardo Saccenti
Dept. of Engineering and Architecture
University of Parma
Parma, Italy
leonardo.saccenti@unipr.it

Jessica Ferrari
Dept. of Engineering and Architecture
University of Parma
Parma, Italy
jessica.ferrari@unipr.it

Daniel Pinardi
Dept. of Engineering and Architecture
University of Parma
Parma, Italy
daniel.pinardi@unipr.it

Angelo Farina
Dept. of Engineering and Architecture
University of Parma
Parma, Italy
angelo.farina@unipr.it

***Abstract*—Kundt's tube and reverberant chamber are common methods for determining the sound absorption coefficient or acoustic impedance of materials. These measurement methodologies are well-known and standardized, albeit not being practicable in-situ and requiring the isolation of samples of the material under test. Furthermore, Kundt's tube results are affected by sample size, diameter, and length of the tube itself, while reverberant chamber ones by the room dimensions and diffusiveness. In literature, noncontact techniques for sound absorption coefficient and acoustic impedance measurement are widely debated. In this paper, three different noncontact systems for the measurement of the sound absorption coefficient have been investigated: a pressure-velocity probe, a Laser Doppler Vibrometer, and a spherical microphone array featuring 64 capsules. The three methods have been evaluated through in-situ measurements of materials with known acoustic characteristics: Basotect G+ and Expanded Polystyrene. Furthermore, the results obtained with the standard test signal, i.e., white noise, are compared with the exponential sine sweep technique, which provides an increased signal to noise ratio, and allows for removing nonlinear high order distortions and acoustic reflections. As a main contribution of this work, it will be shown that microphone arrays are an optimal solution for measuring the sound absorption coefficient.**

Keywords—Ambisonics, laser doppler vibrometer, microphone array, noncontact measurement, pressure-velocity probe, sound absorption coefficient alpha

I. INTRODUCTION

Acoustical properties of an environment like reverberation time, speech transmission index (STI), or loudness level may have a significant impact on the listening experience. They can cause discomfort, reduce the attention and learning ability, and result in a negative user experience. Sound absorbers or diffusers are commonly employed to reduce the reverberation and to uniformly distribute the sound energy in a closed space. Hence, an accurate evaluation of the acoustic properties of materials, such as the sound absorption coefficient and the acoustic impedance, is more and more important for the design of buildings, passive noise reduction treatments, but also cars [1]–[3] or theatres [4].

The characteristics of these passive acoustics elements are obtained through the acoustical characterization of material samples. The standardized measurement methods the Kundt tube, ISO 10534-2 [5], and the reverberant room, ISO 354 [6]. Although these techniques represent the reference, some important aspects must be considered. As described in [7], [8], Kundt's tube measurements are significantly affected by the sample size, and by the diameter and the length of the tube. Also, the mounting condition of the sample and the air gap between it and the support can affect its vibrational modes and resonances [9]. Although the ISO-354 specifies the reverberant room as an alternative method to the Kundt's tube, other factors affect the estimation of sound absorption coefficients. Most notably, ISO-354 measures the average random-incidence absorption while the Kundt's tube measures the normal incidence absorption and impedance. Additionally, the room's size and diffusiveness can have an impact on the measurement results reducing the reproducibility [10]. Both methods require a small portion of the material under test (MUT), usually an invasive operation since cutting or coring the material is necessary. Furthermore, their applicability is problematic whenever the items to be measured cannot be touched or altered in any way, e.g., historical objects (ancient walls or frescos), or the coring may be impossible, such as for very hard materials, and in all those cases for which the dismantling of the material from the environment would affect its acoustic characteristics.

For the above reasons, several in-situ, noncontact measurement techniques were developed in recent years [11]–[14]. These methods retrieve the sound absorption coefficient and the impedance from the sound pressure and/or particle velocity on the surface of a material. Specifically, there are techniques employing only standard microphones to separate the incident and the reflected wave [15]–[17], while other techniques make use of a microphone and an anemometer to sample separately the sound pressure and the particle velocity close to the surface [18]–[22]. The velocity component can also be measured by using a Laser Doppler Vibrometer (LDV) [23]–[26].

In this paper, three noncontact methods to measure the normal sound absorption coefficient are discussed and compared: pressure-velocity (PU) probe, microphone-LDV, and a microphone array [27]–[30]. The three methods have been evaluated through in-situ measurements of commercial materials with known composition and acoustic characteristics: a 50 mm thickness Basotect G+ panel (a flexible, open-cell foam made from melamine resin) and a 60 mm thickness Expanded Polystyrene (EPS) panel. Two different kinds of test signals have been employed. The standard white noise, and the exponential sine sweep (ESS) technique [31], which has several advantages: a significant

979-8-3503-1104-4/23/

improvement of the signal to noise ratio (SNR), the separation of the high order harmonic distortions from the linear response, the possibility to cut out the reflections of the environment, making the measurement virtually anechoic, and a reduced measurement time. The PU-probe demonstrated good performance on both materials, while the microphone-LDV method revealed suboptimal, and it did not work on the Basotect G+ panel, being the latter a porous material. Eventually, the microphone array method proved to be very effective for the measurement of the sound absorption coefficient.

The paper is arranged as follows. Section II provides a description of the measurement setup and equipment for each method, Section III defines the calibration procedures and post-processing, while Section IV presents the results. Eventually, conclusions are summarized in Section V.

II. Measurement Methods

A. Pressure-velocity probe

The PU-probe is composed of a miniature microphone which samples the sound pressure, and a double hot wire anemometer for the particle velocity measurement. The probe is mounted on a hand-held support mechanically decoupled from a round shaped loudspeaker. The measurement of the temperature differential between closely spaced wires forms the basis of the particle velocity sensor idea. The two platinum wires which compose the double wire anemometer are heated up to approximately 200 °C. The temperature of the air rises as it passes through the upstream wire, cooling the wire in the process. A voltage differential can be determined as the wires' different temperatures lead to different electrical resistances [32]. Due to the probe characteristics, this method is usually suitable for soft and absorbing materials, and the bandwidth is limited between 200 Hz and 10 kHz.

The PU-probe employed in this work is Microflown PU Regular. The connection scheme can be seen in Fig. 1. A computer is connected to a soundcard (ZOOM F8) to play and synchronously record the test signals. The output of the soundcard feeds an analog amplifier (QSC CX168) connected to the loudspeaker of the probe, while sound pressure and particle velocity are sampled by the signal conditioner, and eventually recorded on the first two channels of the soundcard, both set with an input gain of 30 dB. The Root Mean Square (RMS) value of the output voltage was set to 1 Vrms by using a TrueRMS tester. The distance between the loudspeaker and the sensors is fixed to 26 cm for the Microflown. During the measurement, the distance between the sensors and the surface of the MUT was 1 cm.

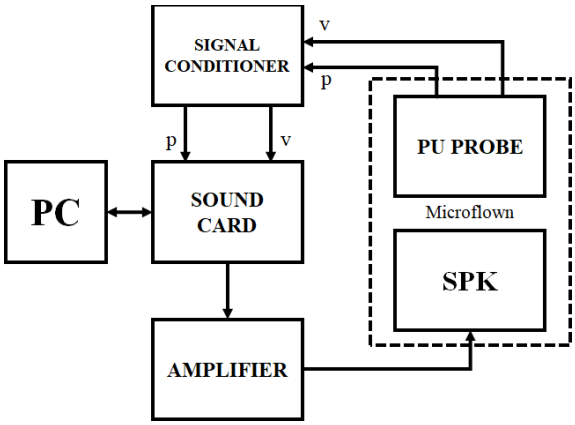

Fig. 1. Microflown measurement setup

B. Microphone and Laser Doppler Vibrometer

The LDV is used as a velocity sensor to sample the vibration velocity of the MUT, while it is excited at a defined distance with a test signal. The LDV acquires mechanical vibration characteristics by employing the heterodyne interferometer technique [33]. The vibrating object is targeted by the laser beam, which is then reflected. Due to the Doppler effect, the velocity of a vibrating object causes a frequency modulation of the laser light. The velocity information is obtained from this frequency modulation. The need for the reflection of the laser light may reduce the effectiveness of this method with open-cell porous materials. A standard microphone, positioned very close to the surface of the material under test, is employed to sample the sound pressure.

The LDV system employed in this work was a VibroGo VG-200 by Polytec. The sensitivity was set to 5 mm/s/V, for a maximum measurement range of 20 mm/s. A built-in high-pass filter was enabled at 13 Hz to remove the low frequency disturbances. The microphone was a laboratory grade one by Bruel&Kjaer (B&K), type 4189 (class 1), having a sensitivity of 50 mV/Pa, half inch dimension, inherent noise of 14.6 dB(A), and working frequency range 6.3 Hz – 20 kHz. The measurement setup is depicted in Fig. 2. A computer is connected to a soundcard (ZOOM F8) to play and synchronously record the test signals. The output of the soundcard feeds the input of an analog amplifier (QSC CX168), connected to a Genelec Studio Monitor type 8351a, a three-way point source with an almost flat frequency response (+/- 1.5 dB in the range 38 Hz – 20 kHz). The output voltage was set to 1 Vrms by using a TrueRMS tester. The B&K microphone and the LDV were recorded by the soundcard on the first two channels, both set with an input gain of 30 dB. The loudspeaker and the LDV were positioned at 1 m distance from the MUT, while the B&K microphone at 1 cm.

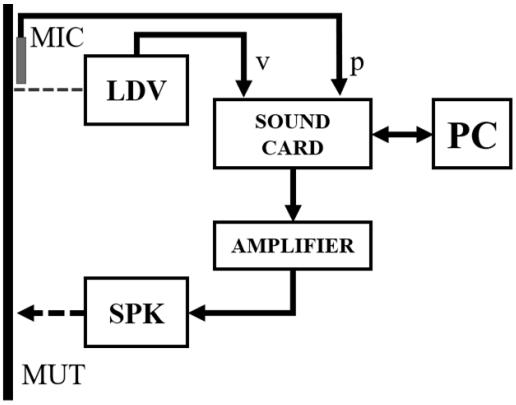

Fig. 2. LDV measurement setup

C. Microphone array

Microphone arrays are nowadays employed for several applications, such as immersive teleconferencing, speakerphone units, virtual or augmented reality (VR/AR) [34], [35], live events streaming, sound field analysis [36]. Their operating principle consists in sampling the sound pressure at the recording point in several positions of the space. Then, the recorded signals are processed to derive a new set of signals, with the aim of encoding the spatial information of the sound field. This operation is called beamforming [37], [38], and the most common format for spatial audio, which is also used in this work, is named Ambisonics [39], [40]. Ambisonics is conceptually obtained

by placing at the observing point several coincident virtual microphones, characterized by directivity patterns corresponding to Spherical Harmonics (SH). These are basis functions with orthonormal properties for the Fourier transform on a sphere [41]. In [42], an explicit formulation of the SH can be found.

The first virtual Ambisonics microphone (SH of order 0) corresponds to an omnidirectional microphone, whose polar pattern is a sphere, usually denoted as W. The second, third, and fourth virtual Ambisonics microphones (SH of order 1) correspond to pressure-gradient, or particle velocity, microphones oriented along Y, Z, and X directions (following the current standard "AmbiX" for channel numbering), and their polar pattern has a "figure-of-8" shape. Hence, the usage of the first and fourth virtual Ambisonics microphones allows for encoding the pressure W (Fig. 3, left) and velocity X (Fig. 3, right) signals, which can be used for calculating the sound absorption coefficient.

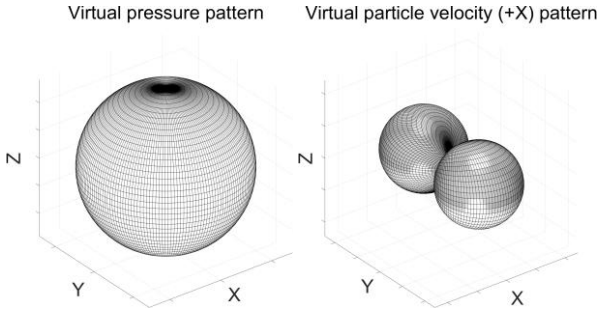

Fig. 3. Virtual pressure microphone (left) and virtual particle velocity microphone (right).

In this work, a commercial microphone array was employed, the Eigenmike-64. It features 64 electret capsules arranged over a rigid sphere of 84 mm diameter. A reader familiar with the subject will have already noticed the array is small if compared to the wavelength at very low frequencies. For this reason, it is expected to get a progressive reduction of accuracy from 500 Hz and below. The schematic for the microphone array measurement can be seen in Fig. 4. A computer is connected to an RME Digiface Dante sound card via Universal Serial Bus (USB). The sound card receives the 64 pressure channels from the array and transmits synchronously the test signal to the loudspeaker through the analog out of a Dante amplifier. The loudspeaker is the Genelec Studio Monitor previously described (see Section II-*B*). The output voltage was set to 1 Vrms by using a TrueRMS tester. The loudspeaker was positioned at 1 m distance from the MUT, while the array at 1 cm.

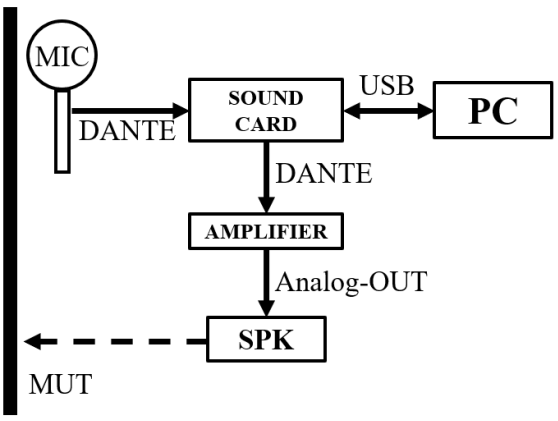

Fig. 4. Measurement schematic with spherical microphone array.

III. Post-processing and Calibration

In this Section, the signal processing required for the ESS technique, the microphone array, and the calibration of the measurement systems are described.

A. Exponential Sine Sweep technique

The several advantages of this technique derive from the convolution of the recorded ESS with the inverse ESS. Such operation packs the entire information in a very short time domain signal, named impulse response (IR). One IR is obtained for each recorded channel; hence, two for the PU-probe or microphone-LDV system, and 64 for the microphone array. The ESS technique allows for separating the linear response, which we are interested in, and the high order harmonic distortion components, as shown in Fig. 5. Once the linear response is isolated, a fading window is applied. In Fig. 6, the linear IRs and fading windows for pressure and velocity channels of the PU-probe can be seen as an example. If strong reflections caused by the environment are found, the linear IR can be cut shorter to exclude them, namely virtual anechoic measurement technique. This is a significative advantage with respect to the white noise signal.

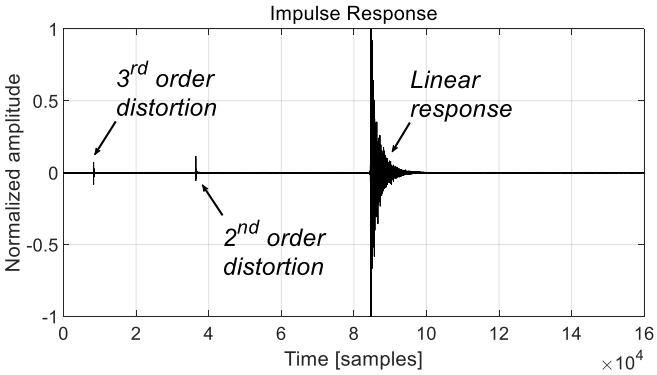

Fig. 5. Time domain Impulse Response with linear response and high distortion orders.

One can note the delay occurring between the zero sample and the main peak of the linear IR corresponds to the travel path of the sound wave in air, calculated as:

$$d = \frac{D}{fs} \cdot c_0 \qquad (1)$$

where D is the delay in samples, fs is the sampling frequency and c_0 is the sound speed. In the case of Fig. 6, that is a Microflown measurement, the values D = 37, fs = 48 kHz, and c_0 = 343 m/s provide a result of d = 26 cm, as expected. Eq. (1) can also be applied to identify the main reflections occurring after the direct sound, where D is the number of samples between the peak of the reflection and the main peak of the IR. In the case of Fig. 6, the reflection occurs at sample 457, hence D = 457-37 = 420. This leads to a sound path equal to 3 meters, which is twice the distance between the PU-probe and the floor/ceiling, being the PU-probe positioned in the middle of a 3 m height laboratory.

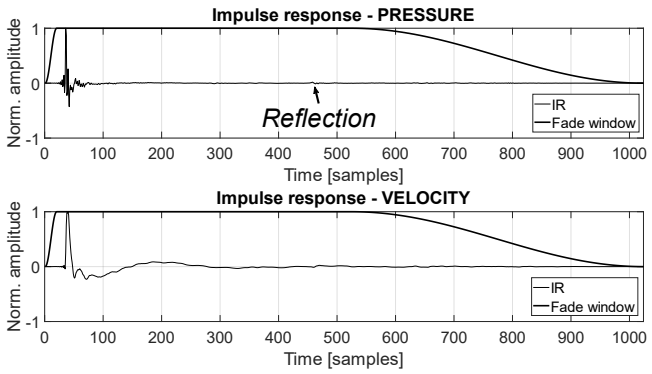

Fig. 6. Time domain linear Impulse Response with fade window for pressure channel (above) and velocity channel (below).

B. Microphone array beamforming

The conversion of the pressure signals recorded by the microphone array into Ambisonics virtual microphones has been performed by means of a linear processing, with a matrix $\boldsymbol{H}$ of Finite Impulse Response (FIR) filters. The FIR filter matrix $\boldsymbol{H}$ is computed in frequency domain with the Kirkeby algorithm [43]:

$$\boldsymbol{H}[k]_{M\times VM} = \boldsymbol{C}[\vartheta,\varphi,k]'_{M\times D}\cdot\boldsymbol{A}[\vartheta,\varphi]_{D\times V}\cdot e^{-j\pi k}\ \cdot \left[\boldsymbol{C}[\vartheta,\varphi,k]'_{M\times D}\cdot\boldsymbol{C}[\vartheta,\varphi,k]_{D\times M}+\beta[k]\cdot\boldsymbol{I}_{M\times M}\right]^{-1} \quad (2)$$

where ϑ the azimuth, φ is the elevation, k is the frequency index, M is the number of capsules (M = 64 for the Eigenmike-64), D is the number of directions, VM is the number of virtual microphones (VM = 2 in this work), $'$ denotes complex conjugate, $^{-1}$ denotes the pseudo-inversion, $\boldsymbol{C}$ is the array response matrix, $\boldsymbol{A}$ is the target directivity matrix, $e^{-j\pi k}$ ensures filter causality, and β is a frequency dependent regularization parameter [44]. The matrix $\boldsymbol{C}$ is obtained by measuring the microphone array with a sound source and two-axis turntable, from hundreds of directions D. Since the characterization of the microphone array is out-of-scope for this work, the authors refer the treatment to previous works [45]–[48]. The target function imposed by the matrix $\boldsymbol{A}$ was defined for this work as the directivity of the first and fourth Ambisonics virtual microphones, respectively sound pressure W and particle velocity along X direction (see Section II-*C* and Fig. 3).

The beamforming matrix $\boldsymbol{H}$ is then converted to time domain, resulting in $\boldsymbol{h}$, by applying an Inverse Fast Fourier Transform (IFFT). Eventually, the recorded pressure signals $\boldsymbol{p}$ are converted in time domain to virtual microphones $\boldsymbol{vm}$ (pressure and velocity) by means of:

$$\boldsymbol{vm} = \boldsymbol{p} * \boldsymbol{h} \quad (3)$$

where $*$ denotes convolution.

C. System calibration

The calibration procedure for PU-probe and microphone array differs from the one for the microphone-LDV system. In the first case, it is possible to perform a free field recording of the test signal, which is instead not possible in the second case, since the LDV does not work in free air but requires a surface to reflect the beam light.

In the case of the PU-probe and microphone array, a free field recording is performed by playing the test signal through the loudspeaker, and by recording it with the microphone and anemometer in the case of the PU-probe, or with the 16 pressure channels with the microphone array. If ESS is employed, the IRs are obtained (see Section III-*A*). In the case of a microphone array, IRs are also convolved with the beamforming matrix $\boldsymbol{h}$, to get pressure and velocity signals (see Section III-*B*). The calibration is then performed by calculating the transfer function H_1 between the pressure and the velocity, as:

$$H_1(f) = \frac{P_{yx}(f)}{P_{xx}(f)} \quad (4)$$

where f denotes the frequency, P_{yx} is the Cross Power Spectral Density (CPSD) between the input signal x (pressure) and the output signal y (velocity), and P_{xx} is the Power Spectral Density (PSD) of the input signal x. The CPSD and PSD were calculated by averaging multiple blocks having a size of 2^{14} samples each, overlapped by 75%, Hann windowed. The transfer function H_1 is converted to time domain by means of an IFFT, thus providing the calibration filter, or "matching filter" h_1, of 2^{14} samples length too. The matching filter h_1 for the PU-probe can be seen in Fig. 7 and Fig. 8, in time and frequency domain, respectively.

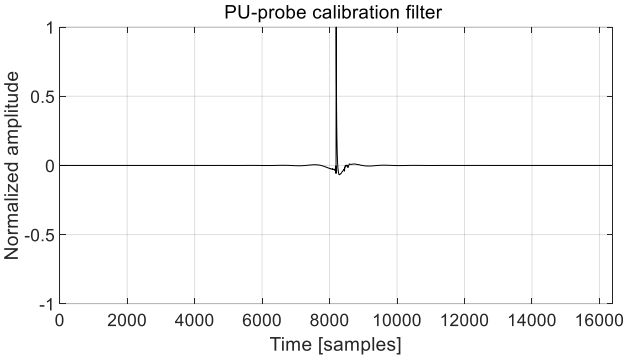

Fig. 7. Matching filter h_1 for PU-probe, time domain.

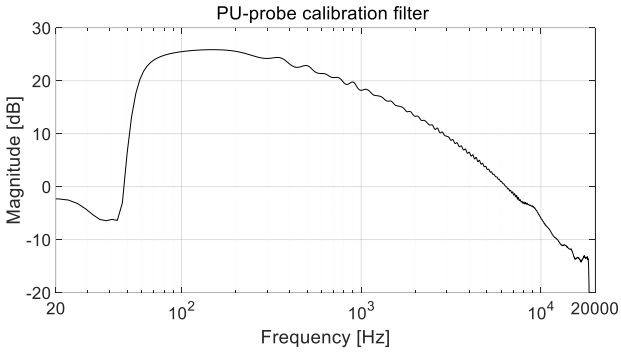

Fig. 8. Matching filter h_1 for PU-probe, frequency domain.

One can note the main peak of the filter occurs at half of its length, that is sample 8192 in this case. Hence, when applied to the velocity signal, the latter gets an initial delay, which must be compensated by delaying the pressure signal of the same number of samples. This can be done by convolving the pressure signal with a centered Dirac's Delta δ (Fig. 9) of the same length as the matching filter. Eventually, the calibration is performed by applying the Dirac's Delta δ to the pressure signal p and the h_1 filter to the velocity signal v, thus resulting in the calibrated pressure p_c and calibrated velocity v_c:

$$p_c = p * \delta \quad (5)$$

$$v_c = v * h_1 \quad (6)$$

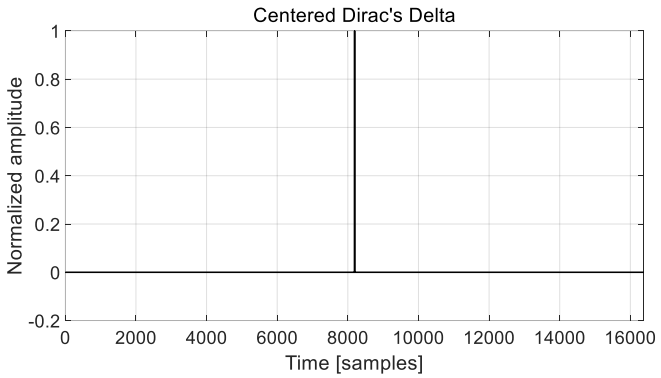

Fig. 9. Dirac's Delta for pressure delay for PU-probe, time domain.

The amplitude calibration of the microphone-LDV system requires recording two calibration signals, separately. The B&K microphone was calibrated with a microphone calibrator (B&K type 4231), which produces a pure tone at 1 kHz, having an RMS value $p_{cal} = 1\ Pa\ (rms)$, that is a Sound Pressure Level (SPL) of 94 dB re 20 µPa. The LDV was calibrated with a vibration calibrator (B&K type 4294), which produces a pure tone at 1000 rad/s (159.2 Hz), having an RMS value $v_{cal} = 0.01\ m/s\ (rms)$, that is a velocity level of 140 dB re 1 nm/s. The amplitude calibration factor $v_{c.f}$ for the LDV is obtained as:

$$v_{c.f} = \frac{v_{cal}}{p_{cal}} \cdot \frac{p_{cal.r}}{v_{cal.r}} \cdot \rho \cdot c_0 \qquad (7)$$

where $p_{cal.r}$ is the RMS value of the sound pressure at the microphone while recording the microphone calibrator, $v_{cal.r}$ is the RMS of the velocity at the LDV while recording the vibration calibrator, $\rho = 1.2\ kg/m^3$ is the density of dry air in standard condition, and $c_0 = 343\ m/s$ is the sound speed in standard condition. In addition, the velocity signal recorded by a LDV system also requires phase correction, which must be proportional to the frequency, as:

$$Z(f) = \frac{k^2(f) + i \cdot k(f)}{1 + k^2(f)} \qquad (8)$$

with *k*:

$$k(f) = \frac{2\pi f \cdot c_0}{d} \qquad (9)$$

where *f* denotes frequency, *i* is the imaginary unit, c_0 is the sound speed (343 m/s), *d* is the distance between the LDV and the MUT (1 m), and *k* is the wave number. The phase correction can be converted into a time domain IR by means of the IFFT, thus providing the phase correction filter *z*, which can be seen for the PU-probe in Fig. 10 (time domain) and in Fig. 11 (frequency domain).

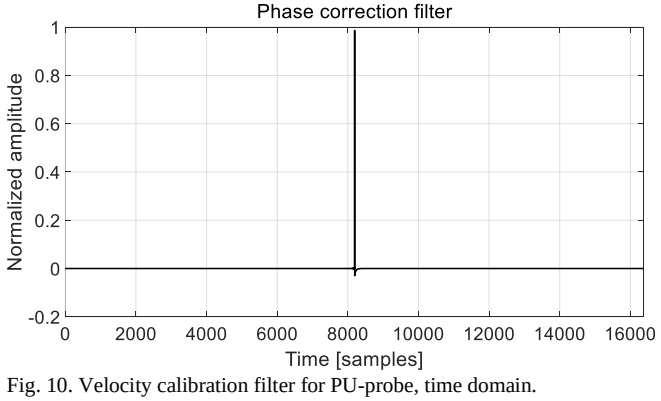

Fig. 10. Velocity calibration filter for PU-probe, time domain.

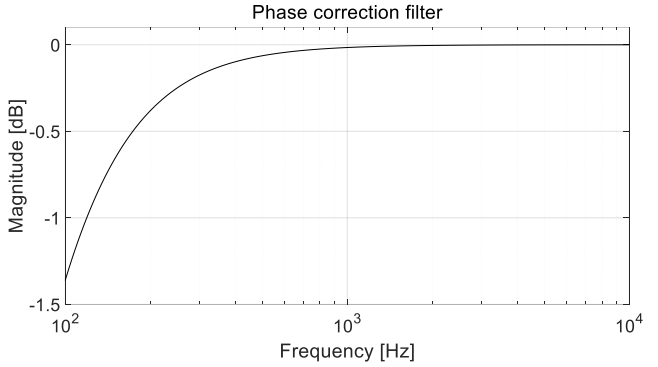

Fig. 11. Velocity calibration filter for PU-probe, frequency domain.

Also in this case, the main peak of the filter occurs at half of its length, hence the pressure signal must be delayed by the same number of samples. Therefore, the calibration is obtained by applying (5) on the recorded pressure signal *p*, while for the velocity *v* it is first required to multiply by the amplitude calibration factor $v_{c.f}$ (7) and then to convolve with the phase correction filter *z*:

$$v_c = (v \cdot v_{c.f}) * z \qquad (10)$$

IV. Experimental Results

The main mechanical characteristics of the measured materials are reported in Table I. They were both tested in the same conditions of temperature and humidity. Each sample was positioned on the floor, first measured ten times in the center point (black dot of Fig. 12) and then eight times moving the test point by two cm around the (squared points in Fig. 12). The texture of the materials can be seen in Fig. 13.

TABLE I. MATERIAL PROPERTIES

Property	***Basotect G+***	***EPS panel***
Dim. (WxLxH) [cm]	100x50x5	100x50x6
Density [kg/m^3]	9	16
Compr. strength [kPa]	≥ 9	≥ 70
Tensile strength [kPa]	≥ 120	≥ 150

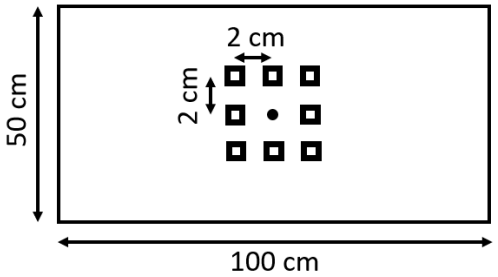

Fig. 12. Measurement schematic for each material sample. Center point (dot) repeated ten times.


Fig. 13. Texture of the measured materials: Basotect G+ (left), EPS (right).

The method employed in this work for calculating the sound absorption coefficient was first introduced by Farina and Fausti in [49], [50]:

$$\alpha(f) = \frac{4 \cdot |Re(P_{yx}(f))|}{Re(P_{xx}(f)) + Re\left(P_{yy}(f)\right) + 2 \cdot |Re(P_{yx}(f))|} \qquad (11)$$

where f is the frequency, P_{yx} is the CPSD, P_{xx} and P_{yy} are the PSD of x and y, and Re denotes the real part. All the results shown in the next paragraph are obtained in 1/3 octave band spectrum. Regarding the test signals, a 120 s length white noise was employed, while the parameters of the ESS were as follows: frequency range 20 Hz – 20 kHz, fade-in 0.5 s, fade-out 0.5 s, length 10 s. One can note the ESS technique allowed for a not negligible reduction of the measurement time.

In the following sections the results for the two materials are shown. The repeatability of the measurement was verified by calculating the maximum variation of the absorption coefficient among the ten measurements repeated on the center point. The maximum variation is obtained by subtracting the minimum value from the maximum value of the ten results, at each frequency. The absorption coefficient curve is obtained by averaging the measurements performed in the eight points around the center.

A. Basotect G+

First, the Basotect G+ was measured with the Microflown PU-probe, results can be seen in Fig. 14 and Fig. 15. One can note the variations are almost negligible with the ESS, particularly at low frequencies where the increase of the SNR provides the highest improvement. Nevertheless, the absorption coefficient alpha is correctly estimated with both methods, despite the ESS being more robust in the frequency range 150 Hz – 500 Hz.

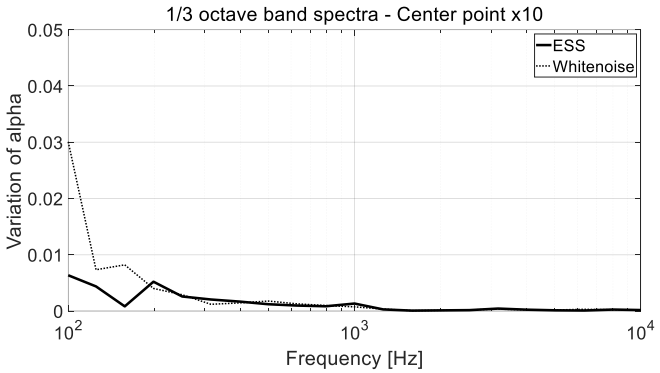

Fig. 14. Basotect G+, variation of the absorption coefficient alpha for ten measurements in the center point, PU-probe.

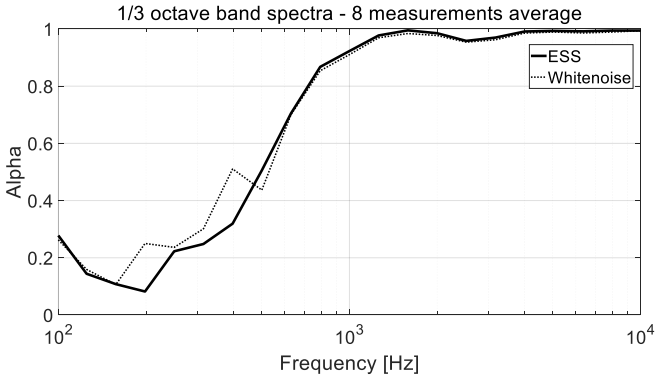

Fig. 15. Basotect G+, average absorption coefficient alpha for eight measurements around the center point, PU-probe.

Then, the Basotect G+ was measured with the microphone-LDV system, results can be seen in Fig. 16 and Fig. 17. Despite an acceptable repeatability, one can note the absorption coefficient is not correctly evaluated by either method, confirming that the LDV cannot be successfully used for porous materials.

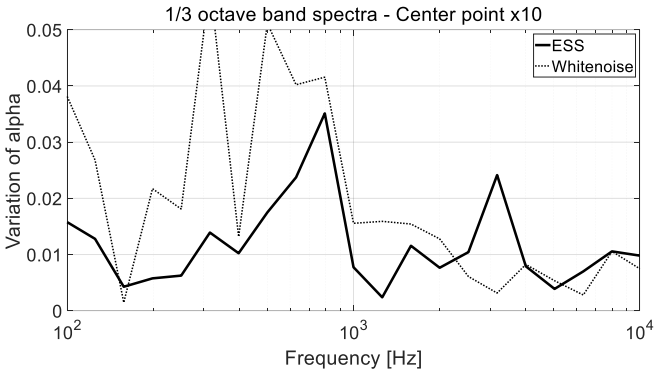

Fig. 16. Basotect G+, variation of the absorption coefficient alpha for ten measurements in the center point, microphone-LDV system.

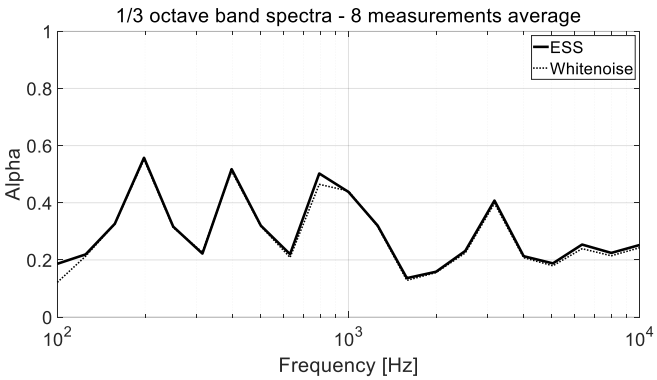

Fig. 17. Basotect G+, average absorption coefficient alpha for eight measurements around the center point, microphone-LDV system.

Eventually, the Basotect G+ was measured with the microphone array, results can be seen in Fig. 18 and Fig. 19. The repeatability of the measurement is very good with both test signals. White noise showed a tendence to overestimate alpha at low frequency and to underestimate it at high frequency. The ESS correctly measured the absorption coefficient above 300 Hz. As expect (see Section II-*C*), the result is less reliable at lower frequencies due to the reduced size of the employed microphone array.

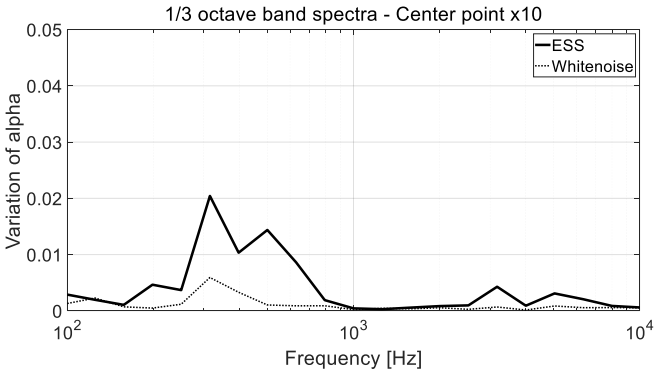

Fig. 18. Basotect G+, variation of the absorption coefficient alpha for ten measurements in the center point, microphone array.

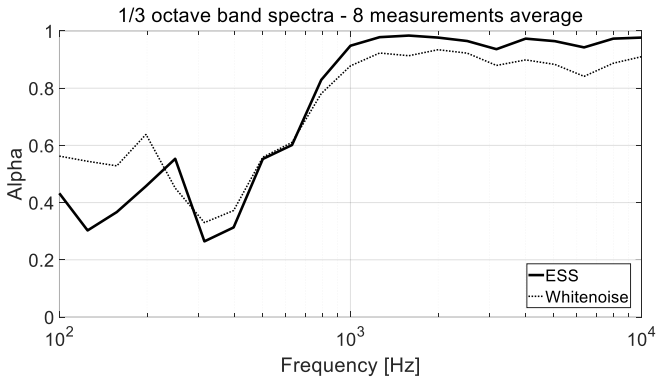

Fig. 19. Basotect G+, average absorption coefficient alpha for eight measurements around the center point, microphone array.

B. Expanded polystyrene (EPS)

First, the EPS panel was measured with the Microflown PU-probe, results can be seen in Fig. 20 and Fig. 21. Also in this case, one can note the variations are almost negligible with the ESS. Despite a trend of underestimating alpha at very low and high frequencies with the white noise can be observed, results are very similar for both test signals.

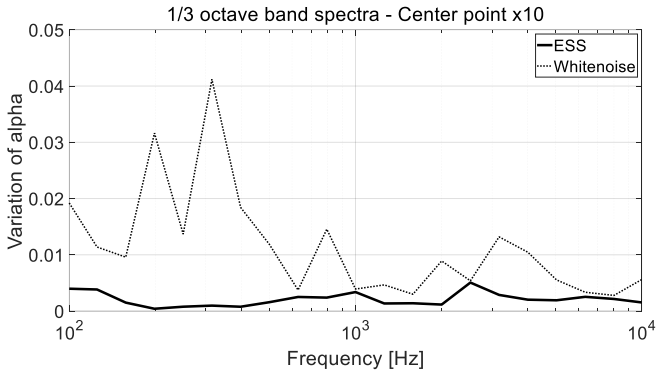

Fig. 20. EPS, variation of the absorption coefficient alpha for ten measurements in the center point, PU-probe.

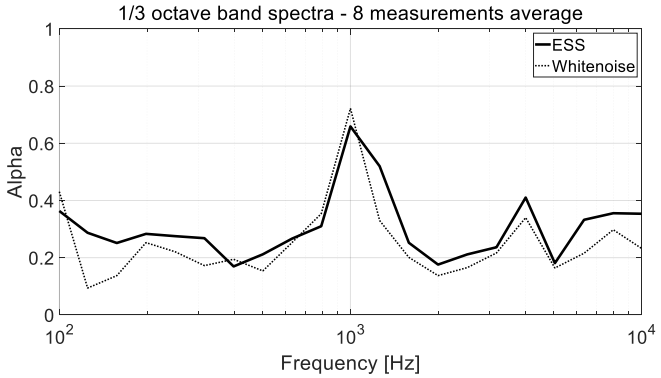

Fig. 21. EPS, average absorption coefficient alpha for eight measurements around the center point, PU-probe.

Then, the EPS panel was measured with the microphone-LDV system, results can be seen in Fig. 22 and Fig. 23. One can note the repeatability is very good with both test signals, and the estimation of alpha almost identical. The absorption coefficient is correctly evaluated in the frequency range 400 Hz – 4 kHz, while it resulted significantly underestimated at lower and higher frequencies.

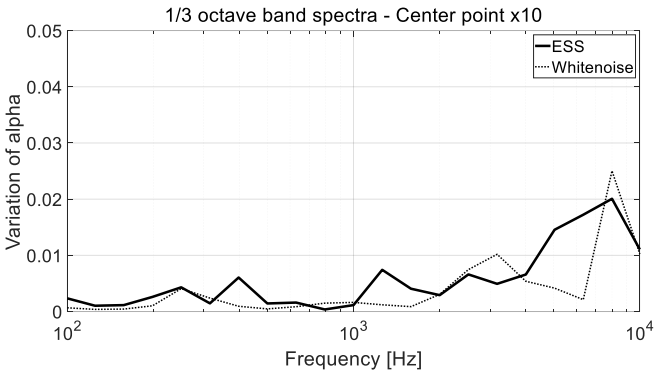

Fig. 22. EPS, variation of the absorption coefficient alpha for ten measurements in the center point, microphone-LDV system.

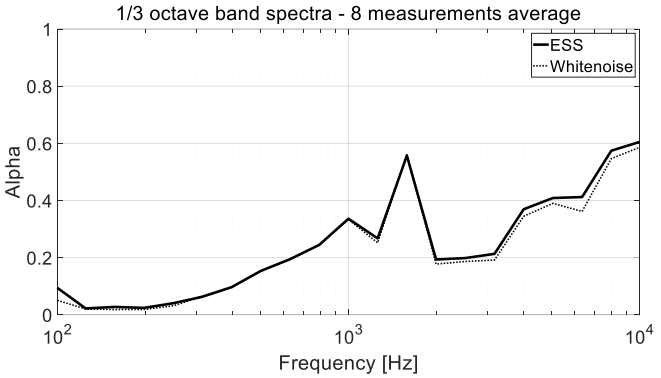

Fig. 23. EPS, average absorption coefficient alpha for eight measurements around the center point, microphone-LDV system.

Eventually, the EPS panel was measured with the microphone array, results can be seen in Fig. 24 and Fig. 25. An excellent repeatability of the measurement is observed with both test signals. The white noise showed a tendence to overestimate alpha at very low frequency, where the SNR is very poor. However, the absorption coefficient estimation is very close to the PU-probe result.

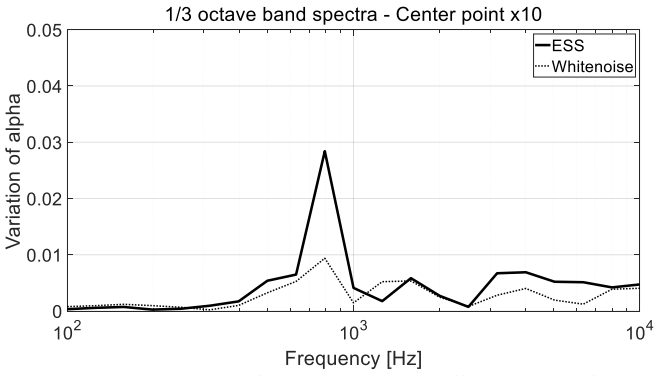

Fig. 24. EPS, variation of the absorption coefficient alpha for ten measurements in the center point, microphone array.

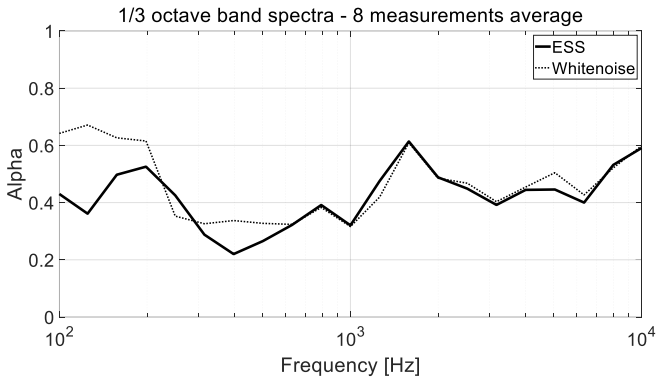

Fig. 25. EPS, average absorption coefficient alpha for eight measurements around the center point, microphone array.

V. Conclusions

Three noncontact techniques for measuring the acoustic absorption coefficient were compared: PU-probe, microphone-LDV system, and a microphone array. Two different test signals were employed: white noise, which has already been in use for decades, and the ESS. The latter packs the time domain information in a short Impulse Response, allowing to improve the SNR by tens of dB, remove the non-linearities, and cut the reflections of the measurement environment. The three methods and the two test signals were used for the measurement of two different materials, Basotect G+ and EPS. The acoustic absorption coefficient alpha was estimated by means of the Farina-Fausti formula.

The PU-probe is the current reference method for noncontact, in-situ measurement of sound absorption coefficient, and it is confirmed by the results of this work. It worked correctly with both materials and test signals, although the ESS is highly recommended for its several advantages and the reduced time required for the measurement.

The microphone-LDV did not work on the Basotect G+ panel, since the LDV is not suitable for porous materials, as expected. Instead, the result on the EPS panel was corrected in comparison with the PU-probe in the frequency range 400 Hz – 4 kHz. Despite the reduced cost of a laboratory grade microphone, an LDV system is usually quite expensive, and considering the limited frequency range of correct operation, it turned out to be the least convenient.

The microphone array technique is the most promising, besides the greater contribution of the presented work. It performed well with both test signals and materials, and particularly with the Basotect G+. The ESS provided more reliable results at low frequency, where the measurement benefits of an increased SNR, and at high frequencies, which are usually affected by the reflections of the environment. As for the PU-probe, it allows for free field calibration. The growing availability of microphone arrays on the market makes it possible to find commercial solutions even at reduced cost, of various shapes and number of capsules, suitable for different ranges of applications.

References

[1] F. Bozzoli and A. Farina, “Measurement of the Speech Intelligibility Inside Cars,” in *Audio Engineering Society Convention 113*, Oct. 2002. [Online]. Available: http://www.aes.org/e-lib/browse.cfm?elib=11298

[2] D. Pinardi, A. Farina, and J.-S. Park, “Low Frequency Simulations for Ambisonics Auralization of a Car Sound System,” in *2021 Immersive and 3D Audio: From Architecture to Automotive, I3DA 2021*, 2021. doi: 10.1109/I3DA48870.2021.9610959.

[3] D. Pinardi, K. Riabova, M. Binelli, A. Farina, and J.-S. Park, “Geometrical Acoustics Simulations for Ambisonics Auralization of a Car Sound System at High Frequency,” in *2021 Immersive and 3D Audio: From Architecture to Automotive, I3DA 2021*, 2021. doi: 10.1109/I3DA48870.2021.9610977.

[4] A. Farina, “Acoustic quality of theatres: correlations between experimental measures and subjective evaluations,” *Applied Acoustics*, vol. 62, no. 8, pp. 889–916, 2001, doi: https://doi.org/10.1016/S0003-682X(00)00082-7.

[5] I. S. O. 10534-2, “Acoustics - Determination of Sound Absorption Coefficient and Impedance in Impedance Tubes - Part 2: Transfer-Function Method.” ISO: Geneva, Switzerland, 1998.

[6] I. S. O. 354, “Acoustics - Measurement of sound absorption in a reverberation room.” ISO: Geneva, Switzerland, 2003.

[7] J. F. Allard and P. Delage, “Free field measurements of absorption coefficients on square panels of absorbing materials,” *J Sound Vib*, vol. 101, no. 2, pp. 161–170, Jul. 1985, doi: 10.1016/S0022-460X(85)81212-8.

[8] T. E. Vigran, L. Kelders, W. Lauriks, P. Leclaire, and T. F. Johansen, “Prediction and Measurements of the Influence of Boundary Conditions in a Standing Wave Tube,” *Acta Acustica united with Acustica*, vol. 83, no. 3, pp. 419–423, May 1997.

[9] A. Cummings, “Impedance tube measurements on porous media: The effects of air-gaps around the sample,” *J Sound Vib*, vol. 151, no. 1, pp. 63–75, Nov. 1991, doi: 10.1016/0022-460X(91)90652-Z.

[10] A. Cops, J. Vanhaecht, and K. Leppens, “Sound absorption in a reverberation room: Causes of discrepancies on measurement results,” *Applied Acoustics*, vol. 46, no. 3, pp. 215–232, Jan. 1995, doi: 10.1016/0003-682X(95)00029-9.

[11] N. Hiremath, V. Kumar, N. Motahari, and D. Shukla, “An Overview of Acoustic Impedance Measurement Techniques and Future Prospects,” *Metrology*, vol. 1, no. 1, pp. 17–38, May 2021, doi: 10.3390/metrology1010002.

[12] E. Brandão, A. Lenzi, and S. Paul, “A Review of the In Situ Impedance and Sound Absorption Measurement Techniques,” *Acta Acustica united with Acustica*, vol. 101, no. 3, pp. 443–463, May 2015, doi: 10.3813/AAA.918840.

[13] B. Briere de La Hosseraye, M. Hornikx, and J. Yang, “In situ acoustic characterization of a locally reacting porous material by means of PU measurement and model fitting,” *Applied Acoustics*, vol. 191, p. 108669, Mar. 2022, doi: 10.1016/j.apacoust.2022.108669.

[14] M. Amran, R. Fediuk, G. Murali, N. Vatin, and A. Al-Fakih, “Sound-Absorbing Acoustic Concretes: A Review,” *Sustainability*, vol. 13, no. 19, p. 10712, Sep. 2021, doi: 10.3390/su131910712.

[15] M. Yuzawa, “A method of obtaining the oblique incident sound absorption coefficient through an on-the-spot measurement,” *Applied Acoustics*, vol. 8, no. 1, pp. 27–41, Jan. 1975, doi: 10.1016/0003-682X(75)90004-3.

[16] M. Ottink, J. Brunskog, C.-H. Jeong, E. Fernandez-Grande, P. Trojgaard, and E. Tiana-Roig, “In situ measurements of the oblique incidence sound absorption coefficient for finite sized absorbers,” *J Acoust Soc Am*, vol. 139, no. 1, pp. 41–52, Jan. 2016, doi: 10.1121/1.4938225.

[17] M. Alkmim, J. Cuenca, L. De Ryck, and W. Desmet, “Angle-dependent sound absorption estimation using a compact microphone array,” *J Acoust Soc Am*, vol. 150, no. 4, pp. 2388–2400, Oct. 2021, doi: 10.1121/10.0006566.

[18] G. Huelsz and F. López-Alquicira, “Hot-wire anemometry in acoustic waves,” *Exp Fluids*, vol. 30, no. 3, pp. 283–285, Mar. 2001, doi: 10.1007/s003480000174.

[19] E. Tijs, H.-E. De Bree, and E. Brandão, “High resolution absorption mapping with a pu surface impedance method,” Baltimore, Maryland, 2010, p. 15003. doi: 10.1121/1.3485674.

[20] P. Cats, E. Tijs, and D. F. Comesana, “Exploration of the differences between a pressure-velocity based in situ absorption measurement method and the standardized reverberant room method,” Montreal, Canada, 2013, p. 15140. doi: 10.1121/1.4798958.

[21] M. Li, W. van Keulen, E. Tijs, M. van de Ven, and A. Molenaar, “Sound absorption measurement of road surface with in situ technology,” *Applied Acoustics*, vol. 88, pp. 12–21, Feb. 2015, doi: 10.1016/j.apacoust.2014.07.009.

[22] E. Güven, D. Fernandez-Comesaña, and T. M. Storani, “Sound intensity-based panel noise contribution analysis for improving the acoustic performance of a vehicle interior,” p. 10, 2021.

[23] L. Saccenti, E. Armelloni, A. Farina, A. Bevilacqua, and L. Lavagna, “In-Situ Measurements of Normal Impedance and Sound Absorption Coefficient of Hard Materials by using a Laser Doppler Vibrometer,”

in *153rd Audio Engineering Society Convention 2022*, New York, NY, USA, Oct. 2022, pp. 1–7. [Online]. Available: http://www.aes.org/e-lib/browse.cfm?elib=21913

[24] A. Le Duff, G. Plantier, J. C. Valière, and B. Gazengel, "Acoustic velocity measurement by means of Laser Doppler Velocimetry: Development of an Extended Kalman Filter and validation in free-field measurement," *Mech Syst Signal Process*, vol. 70–71, pp. 832–852, Mar. 2016, doi: 10.1016/j.ymssp.2015.08.020.

[25] L. Collini, A. Farina, R. Garziera, D. Pinardi, and K. Riabova, "Application of laser vibrometer for the study of loudspeaker dynamics," in *Materials Today: Proceedings*, 2017. doi: 10.1016/j.matpr.2017.06.044.

[26] M. C. Bellini, L. Collini, A. Farina, D. Pinardi, and K. Riabova, "Measurements of loudspeakers with a laser doppler vibrometer and the exponential sine sweep excitation technique," *AES: Journal of the Audio Engineering Society*, vol. 65, no. 7–8, 2017, doi: 10.17743/jaes.2017.0017.

[27] D. Pinardi, A. Toscani, M. Binelli, L. Saccenti, A. Farina, and L. Cattani, "Full-Digital Microphone Meta-Arrays for Consumer Electronics," *IEEE Transactions on Consumer Electronics*, p. 1, 2023, doi: 10.1109/TCE.2023.3267836.

[28] N. Rocchi, A. Toscani, G. Chiorboli, D. Pinardi, M. Binelli, and A. Farina, "Transducer Arrays over A^2B Networks in Industrial and Automotive Applications: Clock Propagation Measurements," *IEEE Access*, vol. 9, pp. 118232–118241, Aug. 2021, doi: 10.1109/ACCESS.2021.3106710.

[29] D. Pinardi *et al.*, "An Innovative Architecture of Full-Digital Microphone Arrays Over A^2B Network for Consumer Electronics," *IEEE Trans Consum Electron*, vol. 68, no. 3, pp. 200–208, Aug. 2022, doi: 10.1109/TCE.2022.3187453.

[30] D. Pinardi, "A Human Head Shaped Array of Microphones and Cameras for Automotive Applications," in *2021 Immersive and 3D Audio: From Architecture to Automotive, I3DA 2021*, 2021. doi: 10.1109/I3DA48870.2021.9610879.

[31] A. Farina, "Simultaneous Measurement of Impulse Response and Distortion with a Swept-Sine Technique," in *108th Convention*, Paris, France, 2000, pp. 1–24. [Online]. Available: http://www.aes.org/e-lib/browse.cfm?elib=10211

[32] H.-E. De Bree, *The Microflown E-book*. Online, 2009. Accessed: May 02, 2023. [Online]. Available: https://www.microflown.com/resources/e-books/e-book-the-microflown-e-book

[33] S. J. Rothberg *et al.*, "An international review of laser Doppler vibrometry: Making light work of vibration measurement," *Opt Lasers Eng*, vol. 99, pp. 11–22, Dec. 2017, doi: 10.1016/j.optlaseng.2016.10.023.

[34] A. Farina, D. Pinardi, M. Binelli, M. Ebri, and L. Ebri, "Virtual reality for subjective assessment of sound quality in cars," in *144th Audio Engineering Society Convention 2018*, 2018.

[35] M. Binelli, D. Pinardi, T. Nili, and A. Farina, "Individualized HRTF for playing VR videos with Ambisonics spatial audio on HMDs," in *Proceedings of the AES International Conference*, 2018.

[36] D. Pinardi, L. Ebri, C. Belicchi, A. Farina, and M. Binelli, "Direction Specific Analysis of Psychoacoustics Parameters inside Car Cockpit: A Novel Tool for NVH and Sound Quality," *SAE Technical Papers*, no. 2020, 2020, doi: 10.4271/2020-01-1547.

[37] L. McCormack, S. Delikaris-Manias, A. Farina, D. Pinardi, and V. Pulkki, "Real-time conversion of sensor array signals into spherical harmonic signals with applications to spatially localised sub-band sound-field analysis," in *144th Audio Engineering Society Convention*, Milan, May 2018, pp. 294–303. [Online]. Available: http://www.aes.org/e-lib/browse.cfm?elib=19456

[38] L. McCormack *et al.*, "Applications of spatially localized active-intensity vectors for sound-field visualization," *AES: Journal of the Audio Engineering Society*, vol. 67, no. 11, 2019, doi: 10.17743/JAES.2019.0041.

[39] M. Gerzon, "Ambisonics. Part two: Studio techniques," *Studio Sound*, vol. 17, no. 8, pp. 24–30, Aug. 1975, [Online]. Available: https://www.michaelgerzonphotos.org.uk/articles/Ambisonics%202.pdf

[40] C. Nachbar, F. Zotter, E. Deleflie, and A. Sontacchi, "Ambix—A Suggested Ambisonics Format," Lexington: 3rd Ambisonics Symposium, Jun. 2011.

[41] N. M. Ferres, *An elementary treatise on spherical harmonics and subjects connected with them*. Cornell University Library, 1877.

[42] Angelo Farina, "Explicit Ambix formulas for High Order Ambisonics," Aug. 2017. http://pcfarina.eng.unipr.it/Aurora/HOA_explicit_formulas.htm

[43] O. Kirkeby, F. Orduna, P. A. Nelson, and H. Hameda, "Inverse Filtering in Sound Reproduction," *Measurement and Control*, vol. 26, no. 9, pp. 261–266, Nov. 1993, doi: 10.1177/002029409302600902.

[44] H. Tokuno, O. Kirkeby, P. A. Nelson, and H. Hamada, "Inverse Filter of Sound Reproduction Systems Using Regularization," *IEICE Transactions on Fundamentals of Electronics, Communications and Computer Sciences*, vol. E80-A, no. 5, pp. 809–820, 1997, [Online]. Available: https://www.melaudia.net/zdoc/kirkebyInverseFilter.PDF

[45] A. Farina, S. Campanini, L. Chiesi, A. Amendola, and L. Ebri, "Spatial sound recording with dense microphone arrays," in *AES 55th International Conference*, Helsinki, Finland, 2014, pp. 1–8. [Online]. Available: http://www.aes.org/e-lib/browse.cfm?elib=17362

[46] D. Pinardi, "Spherical Wave Diffraction for Microphone Arrays Operating in Near Field," in *2023 Immersive and 3D Audio: From Architecture to Automotive, I3DA 2023*, Bologna, Sep. 2023.

[47] D. Pinardi, "Spherical t-Design for Characterizing the Spatial Response of Microphone Arrays," in *2021 Immersive and 3D Audio: From Architecture to Automotive, I3DA 2021*, 2021. doi: 10.1109/I3DA48870.2021.9610850.

[48] D. Pinardi and A. Farina, "Metrics for Evaluating the Spatial Accuracy of Microphone Arrays," in *2021 Immersive and 3D Audio: From Architecture to Automotive, I3DA 2021*, 2021. doi: 10.1109/I3DA48870.2021.9610887.

[49] A. Farina and F. Patrizio, "Standing wave tube techniques for measuring the normal incidence absorption coefficient: comparison of different experimental setups," in *Proceedings of the 11th. International FASE Symposium*, Valencia, 1194, pp. 15–17.

[50] A. Farina and A. Torelli, "Measurement of the Sound Absorption Coefficient of Materials with a New Sound Intensity Technique," Mar. 1997.